Nested Unfolding Network for Real-World Concealed Object Segmentation

Chunming $He^{1,*}$, Rihan $Zhang^{1,*}$, Dingming $Zhang^1$, Fengyang $Xiao^1$, Deng-Ping Fan^2 , and Sina $Farsiu^{1,\dagger}$ ¹Duke University, ²Nankai University,

* Equal Contribution, † Corresponding Author, Contact: chunming.he@duke.edu.

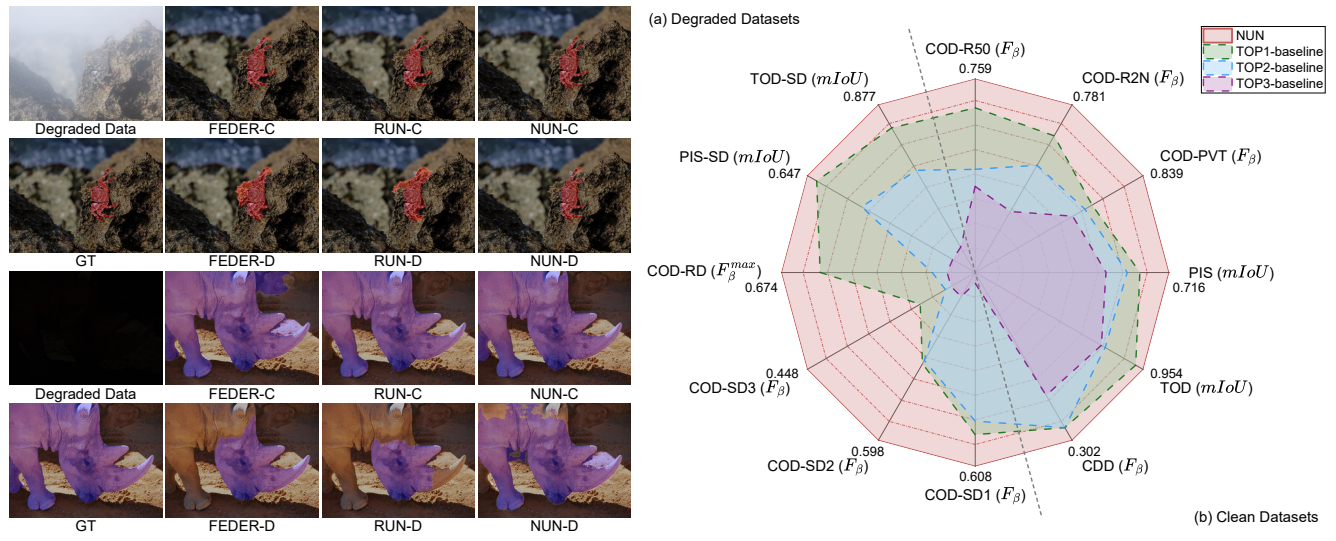


Figure 1. Performance on clean and degraded COS data. Left: Concealed object masks are highlighted in red and purple, overlaid on the original clean data for visual clarity. "-C" and "-D" mean segmentation on clean and degraded samples. Right: The radar chart compares NUN with SOTAs over 12 COS tasks, where TOP1-TOP3 are composite baselines with the top metric scores per task. SD and RD denote synthetic and real-world degradation. Our NUN attains consistently superior results, especially under degradation.

Abstract

Deep unfolding networks (DUNs) have recently advanced concealed object segmentation (COS) by modeling segmentation as iterative foreground-background separation. However, existing DUN-based methods (e.g., RUN) inherently couple background estimation with image restoration, leading to conflicting objectives and requiring predefined degradation types, which are unrealistic in realworld scenarios. To address this, we propose the nested unfolding network (NUN), a unified framework for realworld COS. NUN adopts a DUN-in-DUN design, embedding a degradation-resistant unfolding network (DeRUN) within each stage of a segmentation-oriented unfolding network (SODUN). This design decouples restoration from segmentation while allowing mutual refinement. Guided by a vision-language model (VLM), DeRUN dynamically infers degradation semantics and restores high-quality images without explicit priors, whereas SODUN performs reversible estimation to refine foreground and background. Leveraging the multi-stage nature of unfolding, NUN employs image-quality assessment to select the best DeRUN outputs for subsequent stages, naturally introducing a self-consistency loss that enhances robustness. Extensive experiments show that NUN achieves a leading place on both clean and degraded benchmarks. Code will be released.

1. Introduction

Concealed object segmentation (COS) [4, 5, 10–12, 14, 24–26] aims to delineate objects that visually blend into their surroundings for intrinsic similarities, which is a challenging task requiring detecting subtle foreground–background differences. Despite recent progress, existing COS methods remain vulnerable in real-world scenes, where degradations such as low light and haze obscure discriminative cues and cause localization errors (see Fig. 1). This degradation-affected problem calls for unified modeling of low-level restoration and high-level segmentation.

RUN [17] introduces deep unfolding networks (DUNs) into COS, modeling segmentation as iterative foreground

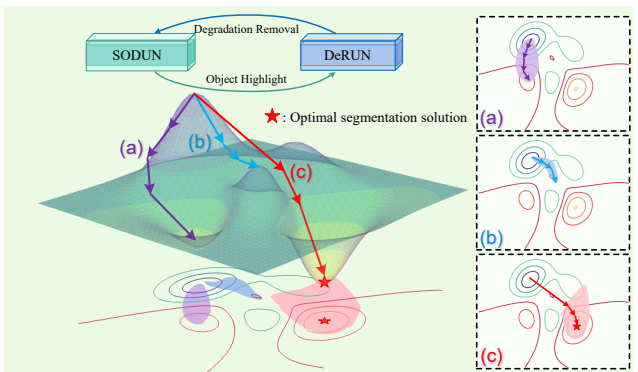


Figure 2. Conceptual motivation of the proposed NUN framework. The blue and purple lines represent restoration-oriented and segmentation-oriented unfolding networks, which correspondingly suffer from task inconsistency and slow convergence. In contrast, the red line indicates our jointly optimized NUN, which bridges the task gap and achieves faster, more stable convergence.

background separation and incorporating image restoration for enhanced robustness. However, its design inherently couples two tasks with conflicting objectives: background estimation emphasizes semantic contrast, while restoration focuses on fine-grained textures. Joint optimization leads to gradient interference and representation entanglement, impairing segmentation accuracy (as discussed in Fig. 2). Moreover, the reliance on predefined degradation types limits adaptability to uncontrolled real-world conditions.

To this end, we propose a nested unfolding network (NUN), a unified and degradation-robust framework for real-world COS. NUN adopts a DUN-in-DUN structure, in which a degradation-resistant unfolding network (DeRUN) is embedded within each stage of a segmentation-oriented unfolding network (SODUN). We employ DUN-based restoration for its interpretable iterative optimization and inherent stability under complex degradations. The multistage formulation enables effective interaction between restoration and segmentation, fostering mutual promotion.

In each stage, SODUN performs reversible foreground-background estimation in both mask and RGB domains, progressively refining semantic and structural details while suppressing false positives and negatives. DeRUN, guided by a vision-language model (VLM) for degradation perception, adaptively estimates descent gradients and restores clean, degradation-free representations without predefined degradation matrices, allowing the outer segmentation DUN to focus on robust high-level cues.

Leveraging the multi-stage property, we introduce the bi-directional unfolding interaction (BUI) that facilitates dynamic information exchange: segmentation outputs guide DeRUN restoration, while high-quality restorations, identified via image quality assessment, are fed back to refine subsequent segmentation stages. To ensure coherent predictions, a cross-stage consistency constraint aligns multi-stage outputs, improving stability and robustness.

Our main contributions are summarized as follows:

- (1) We introduce NUN, a nested unfolding network for real-world COS. This is the first DUN-in-DUN structure for computer vision, enabling joint promotion of image restoration and segmentation within a unified framework.
- (2) We design SODUN for accurate segmentation in a reversible perspective and design a degradation-independent DeRUN guided by VLM for robust restoration under complex and unknown degradation.
- (3) We propose a BUI mechanism that enables mutual guidance between SODUN and DeRUN. Through dynamic feature exchange and cross-stage consistency, BUI enhances interaction and robustness, thus facilitating segmentation.
- (4) Experiments across multiple clean and degraded benchmarks demonstrate that NUN delivers SOTA performance with computational efficiency, validating its generalization ability and scalability to broader vision tasks.

2. Related Works

Concealed object segmentation. Early COS methods, such as SINet [4], ZoomNet [29], and FEDER [10], extend salient object detection frameworks by introducing task-specific modules to extract subtle discriminative cues. However, they assume clean imaging conditions, resulting in severe performance degradation under real-world factors such as haze [7] or low illumination [16]. RUN [17] alleviates this by integrating restoration strategies and formulating COS as an optimization problem via deep unfolding. Yet, its coupling of restoration and background estimation causes optimization conflicts and sensitivity to degradation types, underscoring the need for a degradation-robust structural design—an issue our NUN framework addresses.

Deep unfolding network. DUNs unfold iterative optimization algorithms into learnable multi-stage architectures[15–17], achieving notable success in low-level tasks such as dehazing[7] and illumination enhancement[16]. Recently, their adoption in high-level vision has gained attention. In COS, RUN[17] pioneers this paradigm but assumes fixed degradation conditions, limiting adaptability. In contrast, our NUN introduces a nested architecture where an inner module (DeRUN) performs degradation-agnostic restoration guided by a vision—language model, while an outer module (SODUN) carries out segmentation. This design unifies low- and high-level vision processes in a theoretically grounded and practically robust framework.

3. Models and Optimization

3.1. Image segmentation

$$L(\mathbf{F}, \mathbf{B}) = \frac{1}{2} \|\mathbf{X} - \mathbf{F} - \mathbf{B}\|_{2}^{2} + \beta \varphi(\mathbf{F}) + \lambda \phi(\mathbf{B}), \quad (1)$$

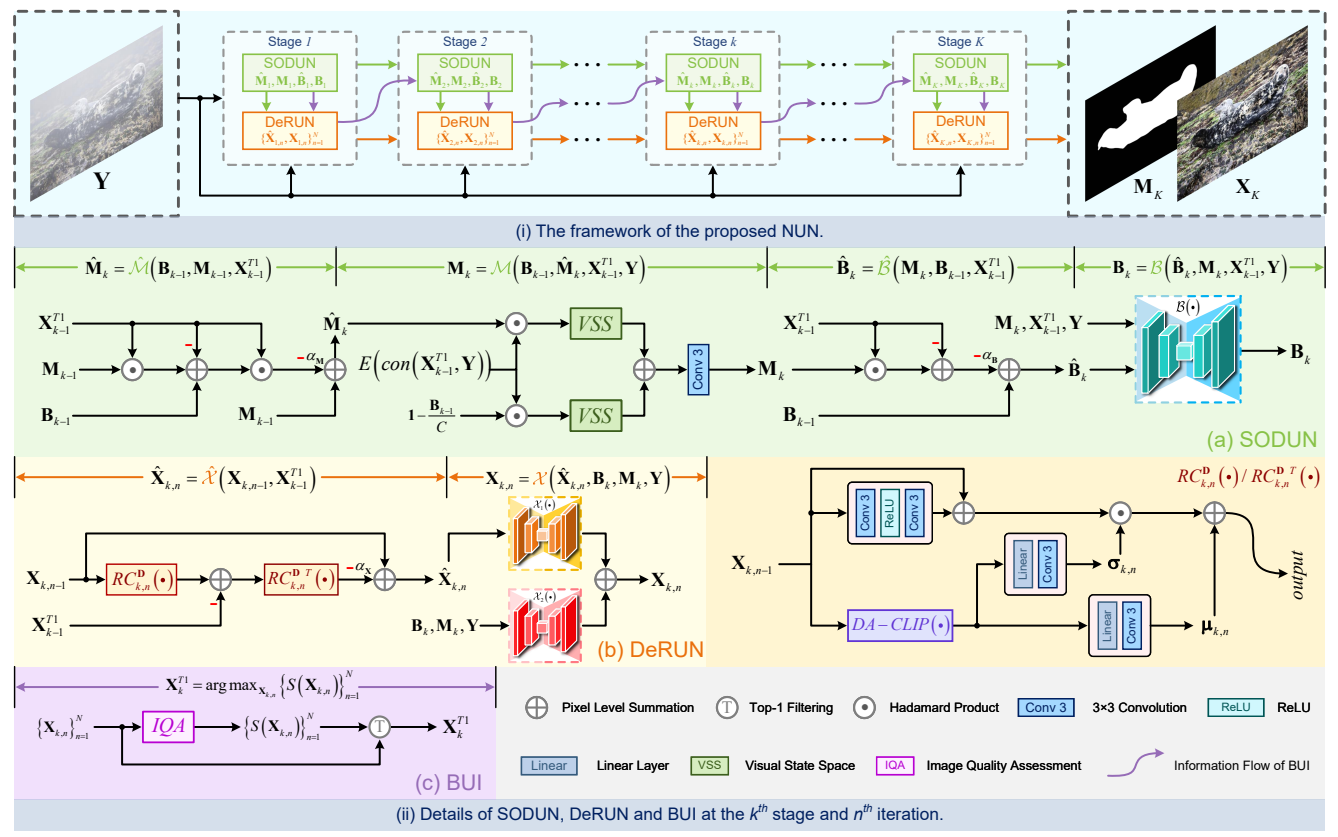


Figure 3. Framework of our proposed NUN.

where $\|\cdot\|_2$ is an ℓ_2 -norm. $\varphi(\cdot)$ and $\phi(\cdot)$ are regularization terms with hyper-parameters β and λ . For segmentation, the foreground is represented as $\mathbf{F} = \mathbf{X} \odot \mathbf{M}$, with \mathbf{M} and \odot denoting the binary mask and dot product, respectively. Substituting into Eq. (1) gives

$$L(\mathbf{M}, \mathbf{B}) = \frac{1}{2} \|\mathbf{X} - \mathbf{X} \odot \mathbf{M} - \mathbf{B}\|_{2}^{2} + \beta \varphi(\mathbf{M}) + \lambda \phi(\mathbf{B}).$$
(2)

Model Optimization. Following the proximal-gradient algorithm [17], we alternately optimize M and B at stage k:

$$\mathbf{M}_{k} = \arg\min_{\mathbf{M}} \frac{1}{2} \|\mathbf{X} - \mathbf{X} \odot \mathbf{M} - \mathbf{B}_{k-1}\|_{2}^{2} + \mu \psi(\mathbf{M}), (3)$$

$$\mathbf{B}_{k} = \arg\min_{\mathbf{B}} \frac{1}{2} \|\mathbf{X} - \mathbf{X} \odot \mathbf{M}_{k} - \mathbf{B}\|_{2}^{2} + \lambda \phi(\mathbf{B}). \quad (4)$$

We first optimize M_k , which consists of a gradient descent term and a proximal term, formulated as:

$$\mathbf{M}_{k} = \mathbf{M}_{k-1} - \alpha_{\mathbf{M}} \nabla m(\mathbf{M}_{k-1}),
= \mathbf{M}_{k-1} - \alpha_{\mathbf{M}} (\mathbf{X} \odot (\mathbf{X} \odot \mathbf{M}_{k-1} + \mathbf{B}_{k-1} - \mathbf{X})),$$
(5)

$$\mathbf{M}_k = \operatorname{prox}_{\mu,\psi}(\hat{\mathbf{M}}_k),\tag{6}$$

where $m(\cdot)$ denotes the data fidelity term of Eq. (3). $\hat{\mathbf{M}}_k$ is the intermediate solution and $\alpha_{\mathbf{M}}$ is a step-size parameter. Similarly, \mathbf{B}_k is optimized with a step-size parameter $\alpha_{\mathbf{B}}$:

$$\hat{\mathbf{B}}_{k} = \mathbf{B}_{k-1} - \alpha_{\mathbf{B}} \nabla b(\mathbf{B}_{k-1}),$$

$$= \mathbf{B}_{k-1} - \alpha_{\mathbf{B}} (\mathbf{B}_{k-1} + \mathbf{X} \odot \mathbf{M}_{k} - \mathbf{X}),$$
(7)

$$\mathbf{B}_k = \operatorname{prox}_{\lambda,\phi}(\hat{\mathbf{B}}_k),\tag{8}$$

where $b(\cdot)$ is the data fidelity term of Eq. (4).

3.2. Image restoration

Restoration Model. Given the degraded observation **Y**, the degradation process can be formulated as:

$$Y = DX + N. (9)$$

where **D** denotes the unknown degradation operator and **N** is the random additive noise. The restoration objective is

$$L(\mathbf{X}) = \frac{1}{2} \|\mathbf{Y} - \mathbf{D}\mathbf{X}\|_{2}^{2} + \gamma \omega(\mathbf{X}), \tag{10}$$

where $\omega(\cdot)$ regularizes the restored image with weight γ . **Model Optimization**. The optimization function of the restoration problem is formulated as:

$$\mathbf{X}_k = \arg\min_{\mathbf{X}} \ \frac{1}{2} \|\mathbf{Y} - \mathbf{D}\mathbf{X}\|_2^2 + \gamma \omega(\mathbf{X}).$$
 (11)

We use the proximal gradient algorithm to optimize the restoration problem with the step-size parameter $\alpha_{\mathbf{X}}$:

$$\hat{\mathbf{X}}_{k} = \mathbf{X}_{k-1} - \alpha_{\mathbf{X}} \nabla x(\mathbf{X}_{k-1}),$$

= $\mathbf{X}_{k-1} - \alpha_{\mathbf{X}} \mathbf{D}^{T} (\mathbf{D} \mathbf{X}_{k-1} - \mathbf{Y}),$ (12)

$$\mathbf{X}_k = \operatorname{prox}_{\gamma,\omega}(\hat{\mathbf{X}}_k),\tag{13}$$

where $x(\cdot)$ is the image fidelity term of Eq. (11).

4. NUN

Motivations. RUN [17] introduces deep unfolding networks (DUNs) into COS by modeling segmentation as it-

Algorithm 1 Proposed NUN Algorithm.

Input: degraded concealed image Y, stage number K, iteration number N

Output: concealed object mask M_K , restored image X_K^{T1} 1: Zero initialization for \mathbf{M}_0 , \mathbf{B}_0 . $\mathbf{X}_0^{T1} = \mathbf{Y}$, $\mathbf{X}_{0.0} = \mathbf{Y}$ 2: for each stage $k \in [1, K]$ do $\hat{\mathbf{M}}_k = \hat{\mathcal{M}}(\mathbf{B}_{k-1}, \mathbf{M}_{k-1}, \mathbf{X}_{k-1}^{T1}),$ $\mathbf{M}_k = \mathcal{M}(\mathbf{B}_{k-1}, \hat{\mathbf{M}}_k, \mathbf{X}_{k-1}^{T1}, \mathbf{Y}),$ $\hat{\mathbf{B}}_k = \hat{\mathcal{B}}\left(\mathbf{M}_k, \mathbf{B}_{k-1}, \mathbf{X}_{k-1}^{T1}\right),\,$ 5: $\mathbf{B}_k = \mathcal{B}\left(\hat{\mathbf{B}}_k, \mathbf{M}_k, \mathbf{X}_{k-1}^{T1}, \mathbf{Y}\right),$ 6: for each iteration $n \in [1, N]$ do 7: $\hat{\mathbf{X}}_{k,n} = \hat{\mathcal{X}}(\mathbf{X}_{k,n-1}, \mathbf{X}_{k-1}^{T1}),$ 8: $\mathbf{X}_{k,n} = \mathcal{X}(\hat{\mathbf{X}}_{k,n}, \mathbf{B}_k, \mathbf{M}_k, \mathbf{Y}),$ 9: 10: $\mathbf{X}_k^{T1} = \arg\max_{\mathbf{X}_{k,n}} \{S(\mathbf{X}_{k,n})\}_{n=1}^N.$ 11:

erative foreground-background separation and embedding restoration methods to handle degraded inputs. However, this design couples background estimation and restoration, whose conflicting goals, semantic suppression versus texture recovery, cause feature entanglement and unstable optimization. Moreover, their reliance on predefined degradation types limits applicability to real-world scenes.

To overcome these issues, we decouple restoration and segmentation into two complementary unfolding processes and adopt DUN for both, leveraging its iterative interpretability and multi-stage stability. Hence, we propose the Nested Unfolding Network (NUN), as shown in Fig. 3 and Algorithm 1. NUN is a unified, degradation-robust framework that adopts a DUN-in-DUN architecture: a degradation-resistant network (DeRUN) nested within a segmentation-oriented network (SODUN). In each stage, SODUN performs reversible foreground–background estimation, while DeRUN restores clean representations guided by a vision–language model (VLM) for degradation perception. A bi-directional unfolding interaction (BUI) further facilitates reciprocal information exchange between segmentation and restoration, forming a closed collaborative loop.

4.1. SODUN

Derived from the segmentation model in Sec. 3.1, SO-DUN takes the degraded image \mathbf{Y} as input. Two modules, $\{\hat{\mathcal{M}}(\bullet), \mathcal{M}(\bullet)\}$ and $\{\hat{\mathcal{B}}(\bullet), \mathcal{B}(\bullet)\}$, simulate the gradient descent and proximal steps for segmentation mask prediction and background estimation, respectively.

Mask prediction. At the k^{th} stage, given \mathbf{B}_{k-1} and \mathbf{M}_{k-1} , the intermediate mask \mathbf{M}_k is obtained as:

$$\hat{\mathbf{M}}_{k} = \hat{\mathcal{M}}(\mathbf{B}_{k-1}, \mathbf{M}_{k-1}, \mathbf{Y}),
= \mathbf{M}_{k-1} - \alpha_{\mathbf{M}}(\mathbf{Y} \odot (\mathbf{Y} \odot \mathbf{M}_{k-1} + \mathbf{B}_{k-1} - \mathbf{Y})).$$
(14)

Eq. (14) strictly follows the proximal gradient derivation, while all fixed parameters are made learnable to enhance

generalization. With the aid of DeRUN, the enhanced result X_{k-1} replaces the low-quality input Y, yielding:

$$\hat{\mathbf{M}}_k = \hat{\mathcal{M}}(\mathbf{B}_{k-1}, \mathbf{M}_{k-1}, \mathbf{X}_{k-1}).$$
 (15)

To further refine $\hat{\mathbf{M}}$, the proximal term adopts a visual state space (VSS) module to capture non-local dependencies, which is essential for global reasoning based on sparse discriminative cues visible in concealed settings. Following common practice [17], we employ deep encoder features $E(\mathbf{X}_{k-1})$ extracted by ResNet50 [19]. To mitigate potential restoration bias, both the restored and original images are utilized. The refined mask \mathbf{M}_k is calculated as:

$$\mathbf{M}_{k} = \mathcal{M}(\mathbf{B}_{k-1}, \hat{\mathbf{M}}_{k}, \mathbf{X}_{k-1}, \mathbf{Y}),$$

$$= conv3(VSS(\hat{\mathbf{M}}_{k} \odot E(con(\mathbf{X}_{k-1}, \mathbf{Y})))$$

$$+VSS((\mathbf{1} - \mathbf{B}_{k-1}/\mathbf{C}) \odot E(con(\mathbf{X}_{k-1}, \mathbf{Y})))),$$

$$+ VSS((\mathbf{1} - \mathbf{B}_{k-1}/\mathbf{C}) \odot E(con(\mathbf{X}_{k-1}, \mathbf{Y})))),$$

$$+ VSS((\mathbf{1} - \mathbf{B}_{k-1}/\mathbf{C}) \odot E(con(\mathbf{X}_{k-1}, \mathbf{Y})))),$$

$$+ VSS((\mathbf{1} - \mathbf{B}_{k-1}/\mathbf{C}) \odot E(con(\mathbf{X}_{k-1}, \mathbf{Y})))),$$

where $con(\cdot)$, $VSS(\cdot)$, and $conv3(\cdot)$ denote concatenation, visual state space, and 3×3 convolution, respectively.

Background estimation. Given M_k and B_{k-1} , the background \hat{B}_k is corrected via the gradient descent step:

$$\hat{\mathbf{B}}_{k} = \hat{\mathcal{B}}(\mathbf{M}_{k}, \mathbf{B}_{k-1}, \mathbf{X}_{k-1}),$$

$$= \mathbf{B}_{k-1} - \alpha_{\mathbf{B}}(\mathbf{B}_{k-1} + \mathbf{X}_{k-1} \odot \mathbf{M}_{k} - \mathbf{X}_{k-1}).$$
(17)

The proximal term refines this estimate using a compact three-layer U-shaped network $\mathcal{B}(\cdot)$ [36]:

$$\mathbf{B}_k = \mathcal{B}(\hat{\mathbf{B}}_k, \mathbf{M}_k, \mathbf{X}_{k-1}, \mathbf{Y}). \tag{18}$$

The degraded–restored pair $\{X_{k-1}, Y\}$ provides valuable degradation-related cues that assist the proximal terms in more precise mask prediction and background correction.

Discussion. By reversibly estimating the foreground and background in both the mask and RGB domains, SO-DUN encourages complementary feedback. This drives the model to focus on ambiguous boundary regions where reciprocal supervision highlights discriminative cues, mitigating false predictions and promoting segmentation results.

4.2. DeRUN

At stage k and iteration n ($1 \le n \le N$), the gradient descent step of DeRUN dynamically adapts to the degradation severity, producing high-quality results $\mathbf{X}_{k,n}$ without relying on any predefined degradation type. To generate the degradation prompt, we use a pretrained CLIP-based VLM, DA-CLIP [27] DA-CLIP(•), to infer degradation semantics, yielding a compact degradation-aware vector $\mathbf{d}_{k,n}$:

$$\mathbf{d}_{k,n} = DA\text{-}CLIP(\mathbf{X}_{k,n-1}),\tag{19}$$

 $\mathbf{d}_{k,n}$ guides the iterative restoration. We employ VLM-informed residual convolutional operators $RC_{k,n}^{\mathbf{D}}(\cdot)$ and $RC_{k,n}^{\mathbf{D}}(\cdot)$ (with a shared structure) to approximate the degradation operator \mathbf{D} and its transpose \mathbf{D}^T [28]:

$$RC_{k,n}^{\mathbf{D}}(\mathbf{X}) = \boldsymbol{\sigma}_{k,n} \odot (CRC(\mathbf{X}) + \mathbf{X}) + \boldsymbol{\mu}_{k,n},$$
 (20)

CHAMELEON CAMO COD10K NC4K Methods Backbones $E_{\phi} \uparrow$ $M \mid$ $F_{\beta} \uparrow$ $E_{\phi} \uparrow$ $S_{\alpha} \uparrow$ $E_{\phi} \uparrow$ $E_{\phi} \uparrow$ $S_{\alpha} \uparrow$ FEDER [10] ResNet50 0.028 0.944 0.892 0.775 0.870 0.802 0.032 0.715 0.892 0.810 0.941 0.069 0.032 **FSEL** [31] ResNet50 0.029 0.847 0.893 0.779 0.881 0.816 0.722 0.891 0.822 0.045 0.807 0.901 0.847 RUN [17] ResNet50 0.027 0.855 0.952 0.895 0.070 0.781 0.868 0.806 0.030 0.747 0.903 0.827 0.042 0.824 0.908 0.851 NUN (Ours) ResNet50 0.026 0.859 0.953 0.899 0.070 0.782 0.883 0.809 0.030 0.759 0.904 0.829 0.042 0.825 0.909 0.852 BSA-Net [38] 0.027 0.851 0.946 0.895 0.079 0.768 0.851 0.796 0.034 0.723 0.891 0.818 0.048 0.805 0.841 Res2Net50 0.956 0.907 0.028 0.914 0.849 0.917 **RUN** [17] Res2Net50 0.024 0.879 0.066 0.815 0.905 0.843 0.764 0.041 0.830 0.859 NUN (Ours) Res2Net50 0.024 0.883 0.957 0.908 0.066 0.822 0.907 0.845 0.027 0.781 0.914 0.849 0.040 0.836 0.918 0.863 CamoDiff [30] 0.952 0.908 **0.042** 0.853 0.936 0.878 0.019 0.815 0.943 0.883 0.028 0.858 0.942 0.895 PVT V2 0.0220.868 RUN [17] PVT V2 0.021 0.877 0.958 0.916 0.045 0.861 0.934 0.877 0.021 0.810 0.941 0.878 0.030 0.868 0.940 0.880 NUN (Ours) PVT V2 0.021 0.888 0.958 0.916 0.042 0.867 0.937 0.019 0.839 0.945 0.886 0.028 0.878 0.942 0.896

Table 1. Results on camouflaged object detection with clean data.

where $CRC(\cdot)$ denotes a Conv-ReLU-Conv block, and $\{\sigma_{k,n}, \mu_{k,n}\}$ are variational parameters:

 $\sigma_{k,n} = conv3(li(\mathbf{d}_{k,n})), \ \mu_{k,n} = conv3(li(\mathbf{d}_{k,n})), \ (21)$ with $li(\cdot)$ being a linear layer. Eq. (20) seamlessly integrates the degradation prompt derived from the VLM into the iterative process. The gradient update at each step is given

$$\begin{split} \hat{\mathbf{X}}_{k,n} &= \hat{\mathcal{X}}(\mathbf{X}_{k,n-1}, \mathbf{X}_{k-1}), \\ &= \mathbf{X}_{k,n-1} - \alpha_{\mathbf{X}} R C_{k,n}^{\mathbf{D}}^{T} (R C_{k,n}^{\mathbf{D}}(\mathbf{X}_{k,n-1}) - \mathbf{X}_{k-1}), \\ \text{where } \mathbf{X}_{k-1} &= \mathbf{X}_{k-1,N} \text{ for brevity. This operation can be} \end{split}$$

interpreted as a progressive removal of residual degradation.

The proximal update is defined as follows:

$$\mathbf{X}_{k,n} = \mathcal{X}(\hat{\mathbf{X}}_{k,n}, \mathbf{B}_k, \mathbf{M}_k, \mathbf{Y}),$$

= $\mathcal{X}_1(\hat{\mathbf{X}}_{k,n}) + \mathcal{X}_2(\mathbf{B}_k, \mathbf{M}_k, \mathbf{Y}),$ (23)

where \mathcal{X}_1 and \mathcal{X}_2 share the same structure as the lightweight network used in background estimation. We introduce the complementary term \mathcal{X}_2 , which leverages segmentation cues to highlight critical structural information and preserve discriminative details during enhancement. Empirically, uncertain and hard-to-segment regions usually correspond to ambiguous pixel-level content; thus, this auxiliary term encourages DeRUN to focus on such challenging areas.

4.3. BUI

BUI exploits the nested structure by encouraging mutual guidance. SODUN masks provide structural priors to DeRUN (via \mathcal{X}_2 in Eq. (23), while DeRUN's outputs are dynamically selected to guide subsequent segmentation.

Given the intermediate outputs $\{X_{k-1,n}\}_{n=1}^{N}$, we employ a comprehensive Image Quality Assessment (IQA) scheme integrating TOPIQ [2], Q-Align [34], and MUSIQ [21] to evaluate perceptual quality:

$$S(\mathbf{X}_{k-1,n}) = IQA(\mathbf{X}_{k-1,n}). \tag{24}$$

The highest quality image, \mathbf{X}_{k-1}^{T1} , is selected to replace \mathbf{X}_{k-1} in all SODUN and DeRUN updates (See Alg. 1).

Although higher-quality restored inputs generally enhance segmentation, a robust framework should remain stable under minor perturbations. Hence, we introduce a cross-stage consistency (CSC) loss, L_{csc} , to enforce con-

sistent predictions between the best and second-best quality inputs, *i.e.*, \mathbf{M}_k (superscript T1 omitted) and \mathbf{M}_k^{T2} at stage k. The formal definition of L_{csc} is provided in Sec. 4.4.

4.4. Loss function

The total loss function is formulated with a parameter ϵ :

$$L_t = L_{basic} + \epsilon L_{csc}, \tag{25}$$

where L_{basic} is the basic loss that jointly supervises segmentation accuracy and image restoration quality. The specific definitions of L_{basic} and L_{csc} are:

$$L_{basic} = \sum_{k=1}^{K} \frac{1}{2^{K-k}} [L_{BCE}^{w}(\mathbf{M}_{k}, GT_{s}) + L_{IoU}^{w}(\mathbf{M}_{k}, GT_{s}) + \|\mathbf{X}_{k} - \mathbf{X}\|_{2}^{2}],$$
(26)

$$L_{csc} = \sum_{k=1}^{K} \frac{1}{2^{K-k}} [L_{BCE}^{w}(\mathbf{M}_{k}, \mathbf{M}_{k}^{T2}) + L_{IoU}^{w}(\mathbf{M}_{k}, \mathbf{M}_{k}^{T2})], \quad (27)$$

where L^w_{BCE} is the weighted binary cross-entropy loss and L^w_{IoU} is the weighted intersection-over-union loss. GT_s and \mathbf{X} denote the ground truth of the mask and clean data. We use \mathbf{X}_k instead of \mathbf{X}_k^{T1} to implicitly encourage the network to generate higher-quality outputs as the iterations progress.

Our loss enables NUN to learn degradation-invariant representations while preserving fine-grained structural fidelity and ensuring stable multi-stage training.

5. Experiment

Experimental setup. Our NUN is implemented in PyTorch and trained on two NVIDIA RTX 4090 GPUs using Adam with momentum terms (0.9, 0.999). Following the common practice [4, 17], we incorporate multi-level deep features extracted from encoder-shaped backbones into our framework. All input images are resized to 352×352 during training and testing phases. The batch size is set to 36, and the initial learning rate is 1×10^{-4} , decreased by a factor of 0.1 every 80 epochs. The stage number K of SODUN is fixed at 4. For the nested DeRUN, its stage number N varies with K, i.e., $N \in \{4, 3, 3, 2\}$ across the four stages.

Table 2. Efficiency comparison with existing cutting-edge methods on COD, where the size of the test image is 352×352 .

Efficiency		R	ResNet50			F	Res2Net50			PVT V2					
Efficiency	FocusDi	ff [37] I	RUN [17]	NUN (Ours)	FEDER	R [10] I	RUN [17]	NUN (O	ırs)	CamoFocus	[22]	RUN [17]	NUN (Ours)	
Parameters (M) ↓	166.	17	30.41	33.17	45.9	92	30.57	35.38		68.85		65.17	65.0	65.67	
FLOPs (G) \downarrow	7618.	.49	43.36	51.72	50.0	03	45.73	54.07	İ	91.35		61.83	70.:	59	
FPS ↑	0.23	3	22.75	20.10	14.0	02	20.26	18.08		9.63		15.82	13.8	36	
Table 3. Resul	lts on clea	n TOD ((GDD).	Table 4.	Table 4. Results on clean PIS (ETIS).					Table 5. Results on clean CDD (<i>CDS2K</i>).					
Methods	mIoU ↑	F_{β}^{max}	\uparrow $M\downarrow$	Methods	n	nDice ↑	mIoU ↑	$S_{lpha}\uparrow$	Me	ethods	$S_{\alpha} \uparrow$	$M\downarrow$	$E_{\phi} \uparrow$	$F_{\beta} \uparrow$	
EBLNet [18]	0.870	0.922	0.064	PolypPVT	`[3]	0.787	0.706	0.871	Hi	tNet [20]	0.563	0.118	0.564	0.298	
RFENet [6]	0.886	0.938	0.057	MEGANe	t [1]	0.739	0.665	0.836	FE	DER [10]	0.538	3 0.070	0.586	0.288	
RUN [17]	0.895	0.952	0.051	RUN [17]		0.788	0.709	0.878	RU	JN [17]	0.590	0.068	0.595	0.298	
NUN (Ours)	0.903	0.954	0.049	NUN (Our	rs)	0.791	0.716	0.880	NU	JN (Ours)	0.595	0.066	0.598	0.302	

Table 6. Results on real-world camouflaged object detection with synthetic degradation data.

		CHAMELEON				1	CA.	мо		<u> </u>	COD10K				NC4K		
Methods	Backbones	$M\downarrow$	$F_{\beta} \uparrow$	$E_{\phi} \uparrow$	$S_{\alpha} \uparrow$	$M\downarrow$	$F_{\beta} \uparrow$	$E_{\phi} \uparrow$	$S_{\alpha} \uparrow$	$M\downarrow$	$F_{\beta} \uparrow$	$E_{\phi} \uparrow$	$S_{\alpha} \uparrow$	$M\downarrow$	$F_{\beta} \uparrow$	$E_{\phi} \uparrow$	$S_{\alpha} \uparrow$
	Single Degradation: Low-Light																
FEDER [10]	ResNet50	0.056	0.721	0.847	0.817	0.130	0.537	0.693	0.636	0.066	0.510	0.742	0.670	0.092	0.619	0.764	0.698
FSEL [31]	ResNet50	0.134	0.221	0.424	0.485	0.175	0.217	0.417	0.462	0.092	0.213	0.518	0.513	0.146	0.253	0.463	0.492
RUN [17]	ResNet50	0.057	0.729	0.841	0.813	0.124	0.579	0.737	0.657	0.063	0.539	0.785	0.684	0.089	0.643	0.795	0.713
NUN (Ours)	ResNet50	0.054	0.736	0.851	0.824	0.112	0.634	0.754	0.724	0.055	0.608	0.795	0.751	0.072	0.714	0.826	0.794
Single Degradation: Hazy																	
FEDER [10]	ResNet50	0.074	0.641	0.744	0.753	0.134	0.543	0.677	0.656	0.060	0.525	0.722	0.728	0.082	0.675	0.746	0.754
FSEL [31]	ResNet50	0.075	0.643	0.755	0.751	0.144	0.505	0,668	0.623	0.081	0.467	0.721	0.656	0.102	0.596	0.752	0.696
RUN [17]	ResNet50	0.067	0.652	0.769	0.748	0.128	0.547	0.681	0.636	0.059	0.528	0.726	0.731	0.079	0.678	0.754	0.764
NUN (Ours)	ResNet50	0.059	0.706	0.815	0.805	0.120	0.574	0.704	0.685	0.053	0.598	0.780	0.743	0.072	0.699	0.811	0.782
				Combin	ned Deg	radatior	: Low-	Resoluti	on, Lov	v-Light.	, and Ha	ızy					
FEDER [10]	ResNet50	0.129	0.422	0.669	0.563	0.169	0.391	0.591	0.529	0.104	0.322	0.657	0.539	0.147	0.408	0.645	0.554
FSEL [31]	ResNet50	0.136	0.413	0.676	0.559	0.173	0.394	0.579	0.531	0.110	0.317	0.637	0.547	0.150	0.397	0.649	0.547
RUN [17]	ResNet50	0.125	0.457	0.680	0.574	0.169	0.394	0.578	0.533	0.100	0.345	0.664	0.548	0.143	0.547	0.630	0.572
NUN (Ours)	ResNet50	0.071	0.629	0.750	0.729	0.137	0.463	0.619	0.599	0.068	0.448	0.686	0.643	0.096	0.572	0.716	0.681
RUN [17]	PVT V2	0.085	0.599	0.800	0.714	0.142	0.496	0.659	0.614	0.085	0.429	0.712	0.627	0.115	0.543	0.72	0.657
NUN (Ours)	PVT V2	0.028	0.862	0.943	0.890	0.077	0.770	0.846	0.784	0.035	0.732	0.880	0.808	0.048	0.815	0.898	0.838

5.1. Comparative Evaluation

Descriptions of the datasets and metrics are provided in the supplementary materials (Supp). For clean data, DeRUN, same as RUN [17], serves as a module that reconstructs the image given the estimated foreground and background.

5.1.1. COS tasks with clean data

Camouflaged object detection. Following FEDER [10], we assess the performance of our model on COD under three backbones: ResNet50 [19], Res2Net50 [8], and PVT V2 [32]. As shown in Tabs. 2 and 5, our NUN shows superior robustness and generalization capability across all four datasets while maintaining computational efficiency.

Transparent object detection. TOD plays a key role in autonomous driving and scene understanding. As shown in Tab. 3, our NUN surpasses existing methods across all datasets, highlighting its potential to advance vision-based perception systems for autonomous driving.

Polyp image segmentation. We evaluate our approach on polyp image segmentation using the *CVC-ColonDB* and *ETIS* datasets. Following RUN [17], PVT V2 is adopted as

the default encoder. As shown in Tab. 4, our NUN consistently achieves leading performance across all datasets.

Concealed defect detection. We assess the zero-shot generalizability to CDD, with models pre-trained on COD applied to *CDS2K* to segment defects. Adhering to [17], PVT V2 serves as the default backbone. As verified by Tab. 5, our NUN achieves superior performance than others.

5.1.2. COS tasks with degraded data

COD with synthetic degradation. To simulate real-world conditions, we introduce three types of degradation (low-light, hazy, and low-resolution) across four datasets [9, 13, 16] (see details in the Supp) and retrain all competing methods. As shown in Tab. 6 and Fig. 4, FEDER [10] and FSEL [31] suffer performance degradation, while unfolding networks (RUN and our NUN) remain robust. NUN generally outperforms RUN [17] by 7.65% (low-light), 6.90% (hazy), and 20.42% (combined degradation), highlighting strong resilience to real-world corruptions. With the stronger PVT-V2 backbone, NUN achieves further gains, highlighting its practicality and potential for deployment.

Table 7. Results on real-world degraded COD.

Table 8. Results on degraded TOD.

Table 9. Results on degraded PIS.

Methods	P	COD-LQ		MCOD-LQ					
Methods	mIoU ↑	$F_{\beta}^{max}\uparrow$	$M\downarrow$	mIoU ↑	$F_{\beta}^{max} \uparrow$	$M\downarrow$			
FEDER [10]	0.104	0.585	0.481	0.159	0.440	0.438			
FSEL [31]	0.108	0.593	0.463	0.230	0.338	0.453			
RUN [17]	0.102	0.653	0.499	0.045	0.490	0.480			
NUN (Ours)	0.061	0.674	0.657	0.034	0.556	0.522			

Methods		GDD								
Wiethous	mIoU ↑	$F_{\beta}^{max} \uparrow$	$M\downarrow$							
EBLNet [18]	0.786	0.873	0.108							
RFENet [6]	0.835	0.896	0.081							
RUN [17]	0.862	0.920	0.070							
NUN (Ours)	0.877	0.928	0.062							

Methods		ETIS							
Wiethous	mDice ↑	mIoU ↑	$S_{\alpha} \downarrow$						
PolypPVT [3]	0.580	0.511	0.731						
MEGANet [1]	0.667	0.596	0.810						
RUN [17]	0.715	0.638	0.830						
NUN (Ours)	0.722	0.647	0.836						

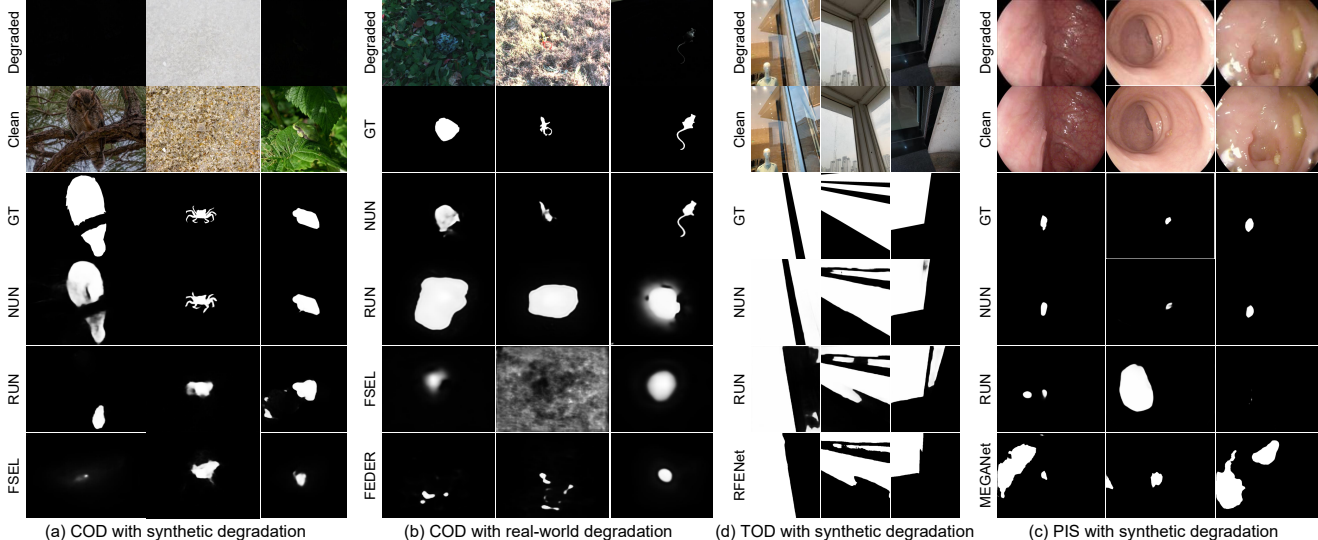


Figure 4. Visualization on COS tasks with real-world and synthetic degradation.

Table 10. Breakdown ablations of NUN.

Table 11. Ablation study of SODUN.

SODUN-	SODUN	DeRUN	BUI	$M \downarrow$	$F_{\beta}\uparrow$	$E_{\phi}\uparrow$	$S_{\alpha} \uparrow$	Metrics	$\hat{\mathcal{M}}_1(\bullet) \rightarrow \hat{\mathcal{M}}(\bullet)$	$\mathcal{M}_1(\bullet) \rightarrow \mathcal{M}(\bullet)$	$\mathcal{B}_1(ullet)\! o\!\mathcal{B}(ullet)$	$\mathcal{B}_2({ullet})\! o\!\mathcal{B}({ullet})$	NUN (Ours)
✓	×	×	×	0.102	0.328	0.603	0.583	$M\downarrow$	0.074	0.073	0.068	0.069	0.068
\checkmark	\checkmark	×	×	0.093	0.362	0.619	0.592	$F_{\beta} \uparrow$	0.412	0.416	0.447	0.445	0.448
\checkmark	\checkmark	\checkmark	×	0.076	0.406	0.646	0.618	$E_{\phi} \uparrow$	0.663	0.666	0.687	0.680	0.686
\checkmark	\checkmark	\checkmark	✓	0.068	0.448	0.686	0.643	$S_{\alpha} \uparrow$	0.630	0.628	0.641	0.639	0.643

COD with real degradation. To evaluate real-world generalization, we invite four annotators to build two low-quality subsets, *PCOD-LQ* and *MCOD-LQ*, from *PCOD* [33] and *MCOD* [23], yielding 160 high-consensus samples (*PCOD-LQ*: 90; *MCOD-LQ*: 70). See Supp for more details. Models pre-trained on COD datasets with combined synthetic degradation are directly tested on the two datasets. As shown in Tab. 7 and Fig. 4, NUN achieves the best results, validating strong generalization to real degradations and the realism and effect of our synthetic degradation design.

Other COS tasks with synthetic degradation. We further extend our evaluation by introducing synthetic degradations into other COS tasks. We add different types of degradation to different tasks, accommodating their specific scenarios (see Supp.). All competing methods are retrained. As reported in Tabs. 8 and 9 and Fig. 4, our NUN achieves the best performance across all datasets, demonstrating its robustness and adaptability to diverse degradation scenarios.

5.2. Ablation Study

Unless otherwise specified, experiments of Secs. 5.2 and 5.3 are conducted on *COD10K* under combined synthetic

degradations, including low-resolution, low-light, and hazy. Please see the ablations for the stage numbers in the Supp.

Effect of SODUN. As shown in Tab. 10, removing the background estimation part (SODUN-) leads to performance drop. Furthermore, in Tab. 11, we analyze the impact of different architectural modifications: (1) adding extra regularization on Eq. (2) like RUN [17] $(\hat{\mathcal{M}}_1(\cdot) \to \hat{\mathcal{M}}(\cdot))$, changing the VSS module used in Eq. (16) with a CNN module with similar parameters $(\mathcal{M}_1(\cdot) \to \mathcal{M}(\cdot))$, replacing our simple network with a complex transformer [13] in Eq. (18) $(\mathcal{B}_1(\cdot) \to \mathcal{B}(\cdot))$, and removing Y in Eq. (18) to break the clean-degradation pair. The performance decreases indicate the effect and efficiency of our SODUN.

Effect of DeRUN. The effect of DeRUN is jointly validated in Tabs. 10 and 12. As shown in Tab. 12, several modifications lead to degraded performance: (1) replacing the explicit prior from DA-CLIP in Eq. (22) with implicit prior learned by the networks $(\hat{\mathcal{X}}_1(\bullet) \to \hat{\mathcal{X}}(\bullet))$; (2) replacing the light-weight network in Eq. (23) with more complex DiffIR used by RUN [17] $(\mathcal{X}_3(\bullet) \to (\mathcal{X}_1(\bullet) \& \mathcal{X}_2(\bullet)))$; and (3) removing the segmentation cues in Eq. (23) (w/o $\mathcal{X}_2(\bullet)$). These consistent performance declines highlight the ratio-

Table 12. Ablation study of DeRUN and BUI.

			•				
Metrics		DeRUN			BUI		NUN
Wietrics	$\hat{\mathcal{X}}_1(\bullet) \rightarrow \hat{\mathcal{X}}(\bullet)$	$\mathcal{X}_3(\bullet) \to (\mathcal{X}_1(\bullet) \& \mathcal{X}_2(\bullet))$	w/o $\mathcal{X}_2(ullet)$	w/o $IQA(ullet)$	$IQA_1(\bullet) \rightarrow IQA(\bullet)$	w/o L_{csc}	(Ours)
$M \downarrow$	0.073	0.068	0.071	0.072	0.070	0.071	0.068
$F_{\beta} \uparrow$	0.422	0.452	0.430	0.421	0.435	0.428	0.448
$E_{\phi} \uparrow$	0.659	0.685	0.671	0.655	0.670	0.665	0.686
S \uparrow	0.628	0.640	0.633	0.626	0.636	0.633	0.643

Table 13. Restored LQ data.

Methods	PSNR ↑	FID↓	User Study
Degraded	11.17	95.63	1.17
DiffIR [35]	18.63	81.07	3.58
RUN [17]	15.21	90.12	2.25
DeRUN	18.04	86.21	3.08
NUN	22.37	73.15	3.92

Table 14. Integrating existing methods with different framework. "-Res": using a restoration method for pre-restoration. "-BLO" "-NUN": integrating the method with bi-level optimization (jointly training with a restoration method) [36] or our NUN.

Metrics	FEDER	FEDER-Res	FEDER-BLO	FEDER-NUN	FSEL	FSEL-Res	FSEL-BLO	FSEL-NUN	RUN	RUN-Res	RUN-BLO	RUN-NUN
$M \downarrow$	0.104	0.090	0.082	0.073	0.110	0.093	0.085	0.078	0.100	0.088	0.079	0.070
$F_{\beta} \uparrow$	0.322	0.357	0.382	0.416	0.317	0.373	0.412	0.435	0.345	0.362	0.391	0.432
$E_{\phi} \uparrow$	0.657	0.635	0.660	0.664	0.637	0.652	0.659	0.668	0.664	0.657	0.668	0.673
$S_{lpha}\uparrow$	0.539	0.586	0.617	0.635	0.547	0.573	0.607	0.624	0.548	0.595	0.618	0.638

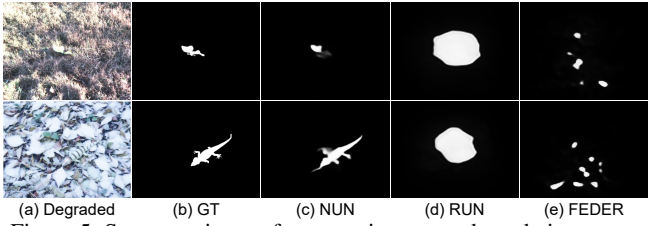


Figure 5. Segmentation performance in unseen degradation types.

(d) RUN (a) Degraded

Figure 6. Image restoration of degraded data.

nality and effectiveness of the proposed DeRUN design. Effect of BUI. The BUI module is designed to enhance information exchange within the DUN-in-DUN architecture. As shown in Tabs. 10 and 12, both components, the IQA-based data selection strategy $(IQA_1(\cdot))$, which relies solely on MUSIQ for evaluation, similar to CORUN[7]) and the consistency loss, contribute to performance improvement. They verify the superiority of our BUI module.

5.3. Further Analysis and Applications

Results on generalization to incomplete supervision and salient object detection are provided in the Supp.

Performance on unseen degradation types. Our NUN trained on synthetic degradations generalizes well to real-world scenarios with diverse and unseen degradation types. As shown in Tab. 7 and Fig. 5, NUN is robust to unseen degradation, like over-exposure and snow.

Image restoration quality. As shown in Tab. 13 and Fig. 6, NUN achieves top results, with a user study containing 12 subjects. In degraded COS, RUN [17] integrates DiffIR [35] as its restoration backbone, yet its performance drops due to conflicts between restoration and segmentation goals. In contrast, NUN alleviates such conflicts and surpasses both

lessly integrated into conventional networks (FEDER and FSEL) by replacing NUN's segmentation branch, and an unfolding-based model (RUN) that embeds DeRUN within each unfolding stage. Results in Tab. 14 reveal consistent performance gains, verifying our scalability and flexibility.

DiffIR and the standalone DeRUN, confirming its ability to jointly enhance restoration and segmentation. Integration with existing models. NUN can be seam-

Potential to serve as a unified vision system. Existing

strategies for real-world high-level vision tasks often rely on pre-enhancement or joint optimization schemes such as bi-level optimization (BLO) [36] and the unfolding-based integration (RUN). While BLO promotes task-specific optimization, and RUN attempts to balance segmentation and restoration objectives, both remain inferior to our unified formulation (Tab. 14). Our experiments demonstrate that NUN not only attains superior segmentation and restoration results (Tab. 13 and Fig. 6) but also achieves mutual enhancement between the two.

6. Conclusions

We introduced NUN for real-world COS, which unifies image restoration and segmentation within a principled framework. By nesting DeRUN within SODUN and using VLM for degradation reasoning, NUN achieves strong robustness under diverse real-world degradations while maintaining efficiency. Experiments validate that NUN is a new SOTA in both clean and degraded scenes, revealing the potential of nested unfolding for broader visual perception tasks.

References

- [1] Nhat-Tan Bui, Dinh-Hieu Hoang, Quang-Thuc Nguyen, Minh-Triet Tran, and Ngan Le. Meganet: Multi-scale edgeguided attention network for weak boundary polyp segmentation. In WACV, pages 7985–7994, 2024. 6, 7
- [2] Chaofeng Chen, Jiadi Mo, Jingwen Hou, Haoning Wu, Liang Liao, Wenxiu Sun, Qiong Yan, and Weisi Lin. Topiq: A top-down approach from semantics to distortions for image quality assessment. IEEE Transactions on Image Processing, 33:2404-2418, 2024. 5
- [3] Bo Dong, Wenhai Wang, Deng-Ping Fan, Jinpeng Li,

- Huazhu Fu, and Ling Shao. Polyp-pvt: Polyp segmentation with pyramid vision transformers. *CAAI Artif. Intell. Res.*, 2, 2023. 6, 7
- [4] Deng-Ping Fan, Ge-Peng Ji, Guolei Sun, Ming-Ming Cheng, and Jianbing Shen. Camouflaged object detection. In CVPR, pages 2777–2787, 2020. 1, 2, 5
- [5] Deng-Ping Fan, Ge-Peng Ji, Ming-Ming Cheng, and Ling Shao. Concealed object detection. *IEEE Trans. Pattern Anal. Mach. Intell.*, 2021.
- [6] Ke Fan, Changan Wang, Yabiao Wang, Chengjie Wang, Ran Yi, and Lizhuang Ma. Rfenet: towards reciprocal feature evolution for glass segmentation. In *IJCAI*, pages 717–725, 2023. 6, 7
- [7] Chengyu Fang, Chunming He, Fengyang Xiao, Yulun Zhang, Longxiang Tang, Yuelin Zhang, Kai Li, and Xiu Li. Real-world image dehazing with coherence-based pseudo labeling and cooperative unfolding network. In *The Thirty-eighth Annual Conference on Neural Information Processing Systems*, 2024. 2, 8
- [8] Shang-Hua Gao, Ming-Ming Cheng, Kai Zhao, Xin-Yu Zhang, Ming-Hsuan Yang, and Philip Torr. Res2net: A new multi-scale backbone architecture. *IEEE Trans. Pattern Anal. Mach. Intell.*, 43(2):652–662, 2019. 6
- [9] Chunming He, Kai Li, and Yulun Zhang. Degradationresistant unfolding network for heterogeneous image fusion. In *ICCV*, pages 611–621, 2023. 6
- [10] Chunming He, Kai Li, Yachao Zhang, Longxiang Tang, and Yulun Zhang. Camouflaged object detection with feature decomposition and edge reconstruction. In CVPR, pages 22046–22055, 2023. 1, 2, 5, 6, 7
- [11] Chunming He, Kai Li, Yachao Zhang, Guoxia Xu, and Longxiang Tang. Weakly-supervised concealed object segmentation with sam-based pseudo labeling and multi-scale feature grouping. *NeurIPS*, 2024.
- [12] Chunming He, Kai Li, Yachao Zhang, Yulun Zhang, Zhenhua Guo, and Xiu Li. Strategic preys make acute predators: Enhancing camouflaged object detectors by generating camouflaged objects. *ICLR*, 2024. 1
- [13] Chunming He, Chengyu Fang, Yulun Zhang, Tian Ye, Kai Li, Longxiang Tang, Zhenhua Guo, Xiu Li, and Sina Farsiu. Reti-diff: Illumination degradation image restoration with retinex-based latent diffusion model. *ICLR*, 2025. 6, 7
- [14] Chunming He, Kai Li, Yachao Zhang, Ziyun Yang, Longxiang Tang, Yulun Zhang, Linghe Kong, and Sina Farsiu. Segment concealed object with incomplete supervision. *IEEE Trans. Pattern Anal. Mach. Intell.*, 2025. 1
- [15] Chunming He, Fengyang Xiao, Rihan Zhang, Chengyu Fang, Deng-Ping Fan, and Sina Farsiu. Reversible unfolding network for concealed visual perception with generative refinement. *arXiv* preprint arXiv:2508.15027, 2025. 2
- [16] Chunming He, Rihan Zhang, Fengyang Xiao, Chengyu Fang, Longxiang Tang, Yulun Zhang, and Sina Farsiu. Unfoldir: Rethinking deep unfolding network in illumination degradation image restoration. *arXiv preprint arXiv:2505.06683*, 2025. 2, 6
- [17] Chunming He, Rihan Zhang, Fengyang Xiao, Chenyu Fang, Longxiang Tang, Yulun Zhang, Linghe Kong, Deng-Ping

- Fan, Kai Li, and Sina Farsiu. Run: Reversible unfolding network for concealed object segmentation. *ICML*, 2025. 1, 2, 3, 4, 5, 6, 7, 8
- [18] Hao He, Xiangtai Li, Guangliang Cheng, Jianping Shi, Yunhai Tong, Gaofeng Meng, Véronique Prinet, and LuBin Weng. Enhanced boundary learning for glass-like object segmentation. In *ICCV*, pages 15859–15868, 2021. 6, 7
- [19] Kaiming He, Xiangyu Zhang, Shaoqing Ren, and Jian Sun. Deep residual learning for image recognition. In CVPR, pages 770–778, 2016. 4, 6
- [20] Xiaobin Hu, Shuo Wang, Xuebin Qin, Hang Dai, Wenqi Ren, Donghao Luo, Ying Tai, and Ling Shao. High-resolution iterative feedback network for camouflaged object detection. In AAAI, pages 881–889, 2023. 6
- [21] Junjie Ke, Qifei Wang, Yilin Wang, Peyman Milanfar, and Feng Yang. Musiq: Multi-scale image quality transformer. In *Proceedings of the IEEE/CVF international conference on computer vision*, pages 5148–5157, 2021. 5
- [22] Abbas Khan, Mustaqeem Khan, Wail Gueaieb, Abdulmotaleb El Saddik, Giulia De Masi, and Fakhri Karray. Camofocus: Enhancing camouflage object detection with split-feature focal modulation and context refinement. In WACV, pages 1434–1443, 2024. 6
- [23] Yang Li, Tingfa Xu, Shuyan Bai, Peifu Liu, and Jianan Li. Mcod: The first challenging benchmark for multispectral camouflaged object detection. arXiv preprint arXiv:2509.15753, 2025. 7
- [24] Shilin Lu, Yanzhu Liu, and Adams Wai-Kin Kong. Tf-icon: Diffusion-based training-free cross-domain image composition. In *Proceedings of the IEEE/CVF International Conference on Computer Vision*, pages 2294–2305, 2023.
- [25] Shilin Lu, Zilan Wang, Leyang Li, Yanzhu Liu, and Adams Wai-Kin Kong. Mace: Mass concept erasure in diffusion models. In Proceedings of the IEEE/CVF Conference on Computer Vision and Pattern Recognition, pages 6430– 6440, 2024.
- [26] Shilin Lu, Zihan Zhou, Jiayou Lu, Yuanzhi Zhu, and Adams Wai-Kin Kong. Robust watermarking using generative priors against image editing: From benchmarking to advances. arXiv preprint arXiv:2410.18775, 2024. 1
- [27] Ziwei Luo, Fredrik K Gustafsson, Zheng Zhao, Jens Sjölund, and Thomas B Schön. Controlling vision-language models for universal image restoration. *arXiv preprint* arXiv:2310.01018, 2023. 4
- [28] Chong Mou, Qian Wang, and Jian Zhang. Deep generalized unfolding networks for image restoration. In CVPR, pages 17399–17410, 2022. 4
- [29] Youwei Pang, Xiaoqi Zhao, Tian-Zhu Xiang, Lihe Zhang, and Huchuan Lu. Zoom in and out: A mixed-scale triplet network for camouflaged object detection. In *CVPR*, pages 2160–2170, 2022. 2
- [30] Ke Sun, Zhongxi Chen, Xianming Lin, Xiaoshuai Sun, Hong Liu, and Rongrong Ji. Conditional diffusion models for camouflaged and salient object detection. *IEEE Transactions on Pattern Analysis and Machine Intelligence*, 2025. 5
- [31] Yanguang Sun, Chunyan Xu, Jian Yang, Hanyu Xuan, and Lei Luo. Frequency-spatial entanglement learning for cam-

- ouflaged object detection. In *ECCV*, pages 343–360, 2024. 5, 6, 7
- [32] Wenhai Wang, Enze Xie, Xiang Li, Deng-Ping Fan, Kaitao Song, Ding Liang, Tong Lu, Ping Luo, and Ling Shao. Pvt v2: Improved baselines with pyramid vision transformer. *Comput. Vis. Media*, 8(3):415–424, 2022. 6
- [33] Xin Wang, Zhao Zhang, and Jun Gao. Polarization-based camouflaged object detection. *Pattern Recognition Letters*, 174:106–111, 2023. 7
- [34] Haoning Wu, Zicheng Zhang, Weixia Zhang, Chaofeng Chen, Liang Liao, Chunyi Li, Yixuan Gao, Annan Wang, Erli Zhang, Wenxiu Sun, et al. Q-align: Teaching lmms for visual scoring via discrete text-defined levels. *arXiv preprint arXiv:2312.17090*, 2023. 5
- [35] Bin Xia, Yulun Zhang, Shiyin Wang, Yitong Wang, Xinglong Wu, Yapeng Tian, Wenming Yang, and Luc Van Gool. Diffir: Efficient diffusion model for image restoration. In *ICCV*, 2023. 8
- [36] Guoxia Xu, Jiangpeng Yan, Longxiang Tang, and Yulun Zhang. Hqg-net: Unpaired medical image enhancement with high-quality guidance. *IEEE Trans. Neural Networks Learn. Syst.*, 2023. 4, 8
- [37] Jianwei Zhao, Xin Li, Fan Yang, Qiang Zhai, Ao Luo, Zicheng Jiao, and Hong Cheng. Focusdiffuser: Perceiving local disparities for camouflaged object detection. In ECCV, pages 181–198, 2024. 6
- [38] Hongwei Zhu, Peng Li, Haoran Xie, Xuefeng Yan, Dong Liang, Dapeng Chen, Mingqiang Wei, and Jing Qin. I can find you! boundary-guided separated attention network for camouflaged object detection. In AAAI, pages 3608–3616, 2022. 5